Published in final edited form as:
Biomaterials. 2012 October ; 33(29): 6943–6951. doi:10.1016/j.biomaterials.2012.06.057.

The alignment and fusion assembly of adipose-derived stem cells on mechanically patterned matrices

Yu Suk Choi[a], **Ludovic G. Vincent**[a], **Andrew R. Lee**[a], **Kyle C. Kretchmer**[c], **Somyot Chirasatitsin**[a], **Marek K. Dobke**[b], and **Adam J. Engler**[a,d]

[a]Department of Bioengineering, University of California, San Diego, CA 92093

[b]Department of Plastic Surgery, University of California, San Diego, CA 92093

[c]Stem Cell Bridges Program, California State University San Marcos, San Marcos, CA 92096

[d]Sanford Consortium for Regenerative Medicine, La Jolla, CA 92037

Abstract

Cell patterning is typically accomplished by selectively depositing proteins for cell adhesion only on patterned regions; however in tissues, cells are also influenced by mechanical stimuli, which can also result in patterned arrangements of cells. We developed a mechanically-patterned hydrogel to observe and compare it to extracellular matrix (ECM) ligand patterns to determine how to best regulate and improve cell type-specific behaviors. Ligand-based patterning on hydrogels was not robust over prolonged culture, but cells on mechanically-patterned hydrogels differentially sorted based on stiffness preference: myocytes and adipose-derived stem cells (ASCs) underwent stiffness-mediated migration, i.e. durotaxis, and remained on myogenic hydrogel regions. Myocytes developed aligned striations and fused on myogenic stripes of the mechanically-patterned hydrogel. ASCs aligned and underwent myogenesis, but their fusion rate increased, as did the number of cells fusing into a myotube as a result of their alignment. Conversely, neuronal cells did not exhibit durotaxis and could be seen on soft regions of the hydrogel for prolonged culture time. These results suggest that mechanically-patterned hydrogels could provide a platform to create tissue engineered, innervated micro-muscles of neural and muscle phenotypes juxtaposed next to each other in order better recreate a muscle niche.

1. Introduction

Regulation of stem cell fate has traditionally relied on presenting small molecules such as growth factors and cytokines in developmentally appropriate ways [1, 2], but such a view omits other important niche characteristics. Biomaterials have recently been used to reproducibly control stem cell differentiation by directly mimicking the niche of the injured or diseased tissues [3–5]; niche mimicry to drive differentiation includes intrinsic extracellular matrix (ECM) cues such as composition [6] and elastic modulus, E, i.e. “stiffness” (measured in kiloPascals, kPa) [7]. A reductionist approach has been used to appreciate the control that each of these properties has on fate, but more recently, properties have been examined in combination. Often cues do not appear additive [8] or at least their

Correspondence to: Adam J. Engler.

combination may be context specific: some ligands support stiffness-induced differentiation whereas others do not [9]. These cues are also rarely static and often presented in spatial or temporal gradients. Stem cells can respond to surprisingly shallow ligand [10] and stiffness gradients [11], emphasizing the need for appropriate spatial control of ECM properties.

Spatial control has often been performed via cell patterning by selectively depositing ECM proteins to allow cell adhesion only on protein-patterned regions, e.g. microcontact printing (μCP) [12]. μCP has been used to control cell area and shape, which can regulate cell membrane tension and ultimately stem cell fate [13, 14]. It can also encourage end-to-end fusion and striation assembly in myoblasts on substrates of myogenic stiffness [15]. However, μCP fidelity relies on maintaining the integrity of the non-fouling region; proteins in serum-containing media, which are often required for stem cells, may deposit over time on soft substrates and decrease pattern fidelity [16]. On the other hand, stiffness alone has been used to show that mesenchymal stem cells become myogenic [17], and specifically for mesenchymal stem cells originating from adipose tissue, i.e. adipose-derived stem cells (ASCs), 2% of cells can even fuse into binucleated myotubes that have lost lineage plasticity [7]. To mechanically regulate where cells reside on a substrate, sequential or photoactivated hydrogel polymerization [18] or photocleavable hydrogels post-polymerization [19] have been used, but these methods have not been applied to study how spatially-controlled stiffness can regulate stem cell fate. In tissues, cell position and fate may be the result of stiffness sorting or other mechanisms [20] with the net result being layers of juxaposed cell layers with different stiffness [21]. In skeletal muscle specifically, cells reside in an aligned ECM comprised of regions with muscle-like stiffness, ~ 10 kPa [15, 17, 22], juxtaposed with regions where softer neurons innervate the firm muscle [23]. Thus, a mechanically patterned substrate with alternating neural and muscle stiffness may be a more physiologically appropriate environment in which to study stem cell myogenesis and encourage cell alignment and end-to-end fusion.

There is also mounting biological evidence that aligning stem cells may promote a more terminally differentiated muscle phenotype. On compliant matrix, cell tractions can propagate over some distance [24] and preferentially align myoblasts over hundreds of microns [15]. Cell-cell adhesion proteins, including M- and N-cadherin, aid cell end-to-end association; function-blocking antibodies for these proteins reduce myoblast fusion [25, 26]. Their expression is also regulated by RhoA [26], implying that spatially regulating cell attachment and alignment could direct expression of these fusion markers and promote fusion by directing traction forces versus unpatterned matrix. With these data in mind, we designed mechanically patterned hydrogels with stripes of alternating stiffness, as well as μCP substrates with the same pattern dimensions. These substrates were used to assess the degree to which different cell types, e.g. neurons, muscle cells, and stem cells, adhered to and sorted on patterned matrices. Stem cell myogenesis was also examined in detail to determine if alignment improved fusion due to a change in fusion-supportive cadherin expression.

2. Materials and methods

2.1 Photolithography and Fabrication of Mechanically-patterned Hydrogels

Mechanically-patterned hydrogel photomasks and molds were created using photolithography. To briefly outline the process illustrated in Fig. 1A *left*, photoresist polymer SU-8 2015 (Microchem) was spin-coated onto a silicone wafer generating ~27 μm thin film. Photomask with alternating black and clear stripes (Zebra pattern) of 100 μm width was placed on top of the photoresist film to selectively polymerize regions of the film, and the wafer was exposed to UV light. The exposed regions remained as a positive feature

(~27 μm in height) after it was developed in a buffer, which washed away non-polymerized photoresist from the wafer.

Mechanically-patterned hydrogel fabrication consisted of a two-step polyacrylamide (PA) hydrogel polymerization process illustrated in Fig. 1A *right*. Acrylamide was polymerized on aminosilanized, 25 mm diameter coverslips (functionalized coverslip) according to the method modified from previously established protocol [27]. Briefly, a gel solution containing the crosslinker N,N′ methylene-bis-acrylamide, acrylamide, 1/100 volume of 10% Ammunium Persulfate and 1/1000 volume of N,N,N′,N′-Tetramethylethylenediamine was mixed. 20 μl of the polymerizing hydrogel solution was sandwiched between the aminosilanized coverslip and a dichlorodimethylsilane (DCDMS)-treated silicone mold made in Fig. 1A *left* to ensure easy detachment. Initial acrylamide/bis-acrylamide solutions were 4%/0.4% and 4.8%/0.4% for neuro-/myogenic and myo-/osteogenic mechanically-patterned hydrogel, respectively. After 15 minutes to allow for polymerization, the hydrogel was detached from the mold, and 15 μl of a second hydrogel solution was added on top of the polymerized hydrogel, covered by a DCDMS-treated coverslip, and polymerized again for 15 min. Input acrylamide/bis-acrylamide solutions for the second layer were 3.2%/0.4% for neuro-/myogenic and 6%/0.4% for myo-/osteogenic mechanically-patterned hydrogel, respectively. After detaching the composite hydrogel from the DCDMS-treated coverslip, mechanically-patterned hydrogel was kept in phosphate-buffered saline (PBS). 10 μg/ml fibronectin [28] or 100 μg/ml type I collagen [29] was chemically crosslinked using a photoactivating crosslinker, Sulfo-SANPAH (Pierce), as indicated. Alternatively, other concentrations of monomer and crosslinker concentrations for the initial and second layers were used, but only when specifically indicated.

2.2 Microcontact printed (μCP) hydrogel

To compare mechanical and protein-based matrix patterns, microcontact printing was used to create alternating protein pattern on static 10kPa gels. PDMS stamps were made from a degased mixture of 10:1 elastomer base to curing agent mixture of Sylgard 184 (Dow Corning) that was poured onto the patterned hydrogel silicon wafers described above and baked for 1 hour at 60°C on a hotplate. Following release from the wafer, the stamps were incubated with a thin film of a 100 μg/ml human plasma fibronectin solution sandwiched between a coverslip and the stamp for 20 minutes. Meanwhile, 10kPa polyacrylamide gels prepared as described above were incubated in a solution of 1mg/ml Sulfo-SANPAH in 50mM HEPES pH 8.5 and placed for 10 minutes under a 4mW/cm^2 350nm UV source. Following three washes in 50mM HEPES pH 8.5, the gels were placed on a hotplate set to 60°C until all remaining solvent had evaporated. PDMS stamps were brought in direct contact with the gels for 10min and a small weight was placed on top of the stamp to ensure good contact between the PDMS microprinting tool and the PA substrate. Hydrogels were peeled from the stamps using tweezers and the resulting substrates immediately immersed in 50mM HEPES pH 8.5 overnight at 37°C.

2.3 Mechanical Force Spectroscopy Mapping by Atomic Force Microscopy

Matrix stiffness was confirmed by atomic force microscopy (AFM; MFP3D, Asylum Research) as detailed previously [27, 30]. Briefly, a pyramidal probe, 0.02 N/m spring constant with a 35° half angle (TR400PB, Olympus), was used to indent a substrate every 25 μm in triplicate over two repeats of the low/high acrylamide-based pattern stripes. Probe indentation velocity was fixed at 2 μm/s with the trigger force of 2 nN. Force spectroscopy was performed over a regular array of spatial coordinates in order to map substrate stiffness over a defined region using the AFM scanning stage (scan size limit of 90 μm × 90 μm); mapping down to 20 nm resolution with this technique is possible as previously shown [31]. Elastic modulus maps were determined by the Hertz cone model with a sample poisson ratio

of 0.5 fit over a range of 10% – 90% indentation force [30]. Surface height and roughness are also simultaneously computed based on when probe deflection occurs as it indents the material. Topographical images were modified using a flattening function to eliminate overall slope from imperfect sample mounting. AFM software (Igor pro 6.22) was applied to generate the force maps, analyze height data, and perform 3D rendering. When applicable, three adjacent maps were assembled together to cover at least two stripes of the alternating pattern.

2.4 Cell isolation and culture

Human ASCs were isolated from freshly aspirated human subcutaneous adipose tissue (donor age between 26 and 31 years) according to the method described previously [32] with approval of UCSD human research protections program (Project #101878). Liposuction samples (300 ml) were washed extensively with equal volumes of phosphate-buffered saline (PBS), and then incubated at 37°C for 45 to 60 min in 0.1% type I collagenase (Worthington Biochemical). Enzyme activity was neutralized with Dulbecco's modified Eagle's medium (DMEM)-low glucose (Invitrogen), containing 10% fetal bovine serum (FBS; Thermo Scientific) and 1% antibiotic/antimyocotic (Invitrogen). Cells were centrifuged at 1200 rpm for 10 min to remove adipocytes. The pellet was resuspended in 0.16 M NH_4Cl and incubated at room temperature for 5 min to lyse red blood cells. Cells were collected by centrifugation at 1200 rpm for 5 min, filtered through a 100 μm cell strainer (BD Falcon) to remove fissile debris, and incubated overnight on tissue culture plastic in complete medium at 37°C and 5% CO_2. Plates were then washed extensively with PBS to remove residual non-adherent cells. To reduce donor-to-donor variation, cells from three different donors were pooled. ASCs were used at low passage numbers between 4 and 8. Morphology was assessed and analyzed using ImageJ software (NIH).

C2C12 skeletal myoblasts (ATCC) were cultured in high glucose DMEM (Invitrogen), 10% FBS and 1% antibiotic/antimyocotic unless cell fusion was induced in which case serum concentration was reduced to 2%. PC-12 cells (ATCC) were cultured in cultured in high glucose DMEM, 10% FBS and 1% antibiotic/antimyocotic.

Chicken embryonic hearts and heart cells were obtained by isolation at 240 hours post fertilization. Animals received humane care in compliance with University of California, San Diego's Institutional Animal Care and Use Committee (protocol #S09200). As detailed elsewhere [33], hearts were obtained by dissection and digested for cell isolation. Isolated hearts were minced using sterile razor blades, washed in PBS and collected with 10 mL of 0.05% trypsin-EDTA (Invitrogen) and incubated in a sterile humidified incubator at 37°C and 5% CO_2 for 15 min. In order to remove red blood cells, the tube was inverted and tissue was allowed to settle prior to a change of solution to 10 ml of fresh trypsin. After 15 min incubation, the sample was centrifuged and the pellet was carefully triturated with normal heart medium containing αMEM (Invitrogen), 10% FBS, and 1% antibiotic/antimycotic. The cell solution was passed through a 70 μm cell strainer and pre-plated on a sterile tissue culture dish for 1 hour at 37°C and 5% CO_2 in order to remove fibroblasts from the solution. The unattached cells were collected, counted, and plated at a density of 10^6 cells/cm^2. Media changes were performed every 2 days.

2.5 Imunocytochemistry, Fusion, and Function blocking Assays

Cells were fixed with 3.7% formaldehyde at room temperature for 15 min. Samples were treated with PBS containing 1% Triton X-100 for 15 min and washed with a washing solution of PBS containing 1 mM $MgCl_2$. The primary antibodies listed below with their indicated dilutions in a staining solution containing 2% bovine serum albumin were then added to samples: α-actinin (1:500; Sigma), MyoD (1:100; Santa Cruz), skeletal myosin

(1:100; Sigma), β tubulin (1:100; Developmental Studies Hybridoma Bank), Ki67 (1:100; eBioscience), and Desmin (1:100; Sigma). Antibodies were incubated with samples for 30 min at 37°C. After washing three times with the washing solution, samples were incubated with Alexa fluor 488- or 568-conjugated secondary antibody (1:400; Invitrogen) for 30 min at 37°C. After washing three times with washing solution, rhodamine phalloidin (1:1000; Invitrogen) stained F-actin for 30 min at 37°C if needed and nuclei were stained by Hoechst 33342 (1:1000; Invitrogen) for 2 min. All samples were examined by a CARV II confocal microscope (BD Biosciences) mounted on a Nikon Eclipse TE2000-U microscope with a motorized, programmable stage using a Cool-Snap HQ camera controlled by Metamorph 7.6 software.

Alternatively, the rabbit polyclonal GC-4 antibody (Sigma) was used to block the function as well as stain N-cadherin depending on whether it was applied chronically to cultures every 48 hours at 40 μmL or during normal staining procedures. For chronic treatment, cell fusion was assessed as described below. ASCs' myotube fusion was confirmed by continuous cytoskeletal structure by staining for β-tubulin and proliferation marker Ki67 to identify and exclude proliferating cells with two nuclei as described previously [7]. To quantify myotube formation frequency, more than 500 nuclei were observed from four independent sample mechanically-patterned hydrogels. Only multi-nucleated cells with continuous cytoskeleton but lack of Ki67 were considered as myotubes. Fusion rate was expressed as the total number of fusion events divided by the total number of nuclei. ASC fusion rate on mechanically-patterned hydrogels was compared to the fusion rate on static 10 kPa hydrogels [7] as well as protein patterned ASCs.

2.6 Statistical analysis

All data are expressed as mean ± standard deviation of experiments from at least four independent repeats. Statistical analysis was performed using student t-test on Graphpad Prism software. P-values < 0.05 were considered to indicate statistical significance.

3. Results

3.1 Mechanically-patterned hydrogel fabrication and characterization

Two different acrylamide concentrations were sequentially polymerized with the first hydrogel polymerized in a micromold and the subsequent one layered on top of the first (see Fig. 1A). This method created a spatially varying stiffness profile of 100 μm–wide stripes in hydrogels; 1 and 10 kPa stripes were produced to make a neurogenic-myogenic mechanically-patterned hydrogel using a small 3.2 to 4% variation in acrylamide concentration with relatively high 0.4% crosslinking bis-acrylamide (Fig. 1B, blue). Stripes approximately of 10 and 34 kPa were made for a myogenic-osteogenic mechanically-patterned hydrogel (Fig. 1B, red) using a 4.8 to 6% variation in acrylamide concentration. However, layering hydrogels of different concentration could introduce differential swelling. To assess substrate height across a neurogenic-myogenic mechanically-patterned hydrogel, both height and stiffness were measured simultaneously by AFM force mapping. Over a 270 μm × 90 μm map, the maximum height range was less than 2 μm, spanning both a soft (dark red) and stiff stripe (Fig. 1C, top; yellow). Mapping indicated that the height difference was most pronounced in a small interfacial region between stripes, but this did not create any appreciable change in surface roughness in this zone or any other, regardless of the stiffness of the pattern (Fig. 1C, bottom). Soft and stiff regions were 80 μm-wide with a 40 μm-wide interface, effectively creating a step gradient in stiffness, since the gradient is 2 orders of magnitude higher than physiological [11]. Compared to controlling hydrogel stiffness by manipulating crosslinker density [34, 35], strategies like the one used here, which employ varying bulk monomer concentration to modulate stiffness in the presence of

a high crosslinker concentration minimize PA hydrogel swelling [36]. Using a lower crosslinker concentration, e.g. 0.1%, resulted in greater differential swelling between layers and created height differences ranging between 8 and 10 μm for 4% and 10% acrylamide layers, respectively, as assessed by AFM force mapping. Larger height differences may induce significant topographical signaling, so only high crosslinker mechanically-patterned hydrogel were investigated further.

To ensure that mechanically-patterned hydrogel stiffness differences did not preclude uniform protein attachment and cell adhesion, both human plasma-derived fibronectin and type I collagen were coated onto the substrates and C2C12 myoblasts were allowed to adhere. No differences in cell adhesion, spreading, or morphology were observed after 48 hours in culture (Supplemental Fig. 1). Stripe pattern was also manipulated to ensure that pattern recognition was independent of pattern geometry. C2C12 myoblasts as well as adipose-derived stem cells (ASCs) were allowed to adhere to mechanically-patterned hydrogels containing 100 μm stiff (10 kPa) and 500 μm soft (1 kPa) stripes or 500 μm stiff (10 kPa) and 100 μm soft (1 kPa) stripes. Both ASCs and C2C12 cells were able to detect the stiffness gradient at the stripe interface and undergo directed migration, i.e. durotaxis [37], towards the stiffer stripes even when cells were up to 250 μm away from the interface (Supplemental Fig. 2). As cells can only sense stiffness and strain differences over tens of microns [15], this phenomenon is likely not due to sensing the interface from such a distance [24] but is rather due to random migration towards the interface prior to the onset of durotaxis.

3.2 Cell adhesion and migration based on mechanical pattern

To assess if the cell clustering on stiffer regions of the substrate observed above was due to preferential adhesion or durotactic migration, C2C12 myoblasts were monitored by time-lapse video microscopy for 24 hours after initial seeding. Cells settled uniformly and attached to the mechanically-patterned hydrogel, but after 1 hour, cell spreading occurred preferentially on the stiffer regions, and by 6 hours, cells began to undergo durotaxis towards stiffer regions (Supplemental Movie 1). Given the variety of contractile cell types that undergo durotaxis, ASCs and cardiomyocytes were also monitored for preferential adhesion and pattern recognition; all three cell types were observed after 48 hours to preferentially attach to stiffer regions of the pattern and, for ASCs and C2C12 myoblasts, align in the direction of the long axis of the pattern (Fig. 2, top and bottom right). Yet again though, cell patterning was not the result of preferential adhesion as cardiomyocytes were evenly distributed and then migrated onto the stripes (Fig. 3A). However for less contractile lineages such as neurons [17], PC12 cells showed no preferential adhesion or migration on either stiffness stripes (Fig. 2, bottom left), consistent with previous observations that these cells have a less spead, more neural phenotype on softer matrix [38].

While pattern fidelity appears to be robust for contractile cell types, it is not clear to what extent mechanical patterning may improve cell patterning versus more commonly used microcontract printing (μCP) methods. Using the same pattern, fibronectin was printed onto 10 kPa hydrogels that lacked the mechanical pattern, and its localization was confirmed immunofluorescently (Fig. 4, left). ASCs seeded onto the μCP pattern initially recognized and attached to pattern, but cells failed to remain on the pattern over time when cultured in serum-containing media (Fig. 4, right). It should be noted that local cell density when pattern recognition became compromised for the μCP pattern was significantly lower than for mechanically-patterned hydrogel (see Fig. 2 and 3 versus 4).

3.3 Improved cell maturation on mechanically patterned matrix

Primary isolated chicken cardiomyocytes were plated onto neurogenic-myogenic mechanically-patterned hydrogel to determine if the pattern would enhance cell alignment and improve cytoskeletal organization. As a result of mechanical pattern of substrate underneath the cells by day 10, cardiomyocytes were aligned along the long axis of stripes and that allowed cell-cell adhesion with alignment; striations were also well aligned along the stripes, with mature striation length of 1.88 ± 0.15 μm found in almost all cells, better than previous reports using unpatterned myocytes [15]. Myofibroblasts (red actin staining only) were also observed by always at the cardiomyocyte periphery (Fig. 3B).

Though relatively mature cardiac cells may reassemble their cytoskeleton on these patterns, it was not clear if undifferentiated stem cells can undergo the same process via lineage specification. Adult stem cells typically undergo a morphology change early in the differentiation process [17], so we first assessed whether cell morphology on mechanically-patterned hydrogels versus stiffness-matched controls was altered. ASCs on mechanically-patterned hydrogel were more elongated with a spindle shape versus cells on unpatterned stiffness-matched hydrogels regardless of culture time (Fig. 5C). Since morphology is only an early and indirect indicator of phenotypic changes, ASC myogenesis was evaluated on neurogenic-myogenic mechanically-patterned hydrogel versus control C2C12 myoblasts. Again both cell types preferentially adhered on stiffer, myogenic stripes at day 1 (Fig. 5A, left). C2C12 myoblasts showed long, fused myotubes at day 7 expressing myoD and skeletal fast myosin (Fig. 5A, right). Myoblast fusion was independent of pattern geometry as fused, desmin positive myotubes could be observed on larger patterns, though alignment was less robust at larger pattern spacing (Supplemental Fig. 3). ASCs also underwent myogenesis, expressing MyoD by day 7 (Fig. 5A, right), despite myotube formation not being as apparent when observed in brightfield (Fig. 5A). Careful inspection with cytoskeletal proteins, however, indicated that ASCs on stripes of myogenic stiffness did in fact form fused, multi-nucleated cells that were negative for the proliferation marker ki67 (Fig. 5B), consistent with previous reports on unpatterned, myogenic matrix [7]. However with the enhanced alignment of cells on patterned versus unpatterned, especially at day 7 (Fig. 5D), we noted that the fusion rate on mechanically-patterned hydrogel was almost twice (3.8 ± 0.3%) as the rate on unpatterned 10 kPa gels (2.0 ± 0.3%) (Fig. 5E, top). Only bi-nucleated myotubes were previously observed from matrix-stiffness induced differentiation, but with the enhanced alignment from mechanically-patterned hydrogel, ASC-derived myotubes with more than 3 nuclei were observed (Fig. 5E, bottom).

4. Discussion

Our ability to regulate cell fate via matrix chemistry and/or mechanics has been well documented [3, 4, 13, 14, 21], and while stem cell hapto- [10] and duro-taxis [11] has been observed via gradients, the effects of precisely patterned matrix on stem cell behavior has not been completely explored. Such precise patterns are commonly found *in vivo*, e.g. skeletal muscle contains layers of aligned myotubes [15, 17, 22] juxtaposed with regions where softer neurons innervate the firm muscle [23]; thus our objective was to develop a hydrogel platform that mimicked *in vivo* ECM stiffness of normal muscle to examine stiffness-based micropatterning's influence on stem cell fate. Relative to μCP patterns, myogenic stiffness patterns remain robust over time and produce cultures of aligned stem cells that fuse at higher rates and with greater numbers of fusing cells than unpatterned matrices. These data implicate matrix-based patterns as means of enhancing ECM-based cell cues, but closer examination of these data is warranted in the broader context of ECM and micropatterning.

4.1 Matrix considerations when micropatterning

While the fidelity of longer-term μCP patterns on compliant hydrogels may by difficult, mechanically-patterned hydrogels also have a unique set of considerations that must be overcome. For example, differential swelling has been reported in microfabricated hydrogels but can be minimized when using substrates with high crosslinker content [36]; here we report the same observation where mechanically-patterned hydrogels can be fabricated with minimal differential swelling, i.e. < 2 μm, and with minimal roughness difference, i.e. < 200 nm, between soft and firm regions when the crosslinker fraction is higher than previously used [11]. The 2-step soft lithography process used in creating the mechanically-patterned hydrogel also makes predicting hydrogel stiffness inherently difficult due to layer diffusion during polymerization. In hydrogels with wider spaced stripes, e.g. the 500 to 100 μm stripe width mechanically-patterned hydrogel, and/or when sequentially polymerized within a single layer [18], stiffness changes from monolayer hydrogels were less appreciable; the amount of monomer and crosslinker from the large second layer was not significantly depleted. Yet with sequentially polymerized small stripes of equal spacing, significant deviations from monolayer hydrogels [11] were evident as depletion may cause noticeable loss of monomer from the second layer. As a result, small changes in monomer, e.g. 4% (bottom) versus 3.2% (top), produce regions with an order of magnitude difference in stiffness. Materials that lack mixing issues, e.g. polydimethylsiloxane (PDMS), may have a more predictable but often limited stiffness range when creating spatial stiffness patterns [39]. However all of these materials appear to have similar ligand binding independent of stiffness, as was observed here with similar cell densities on fibronectin- and type I collagen-coated substrates.

Aside from other materials, stiffness gradients have been created using photoinitiators and masks [11, 40, 41], but significant diffusion and UV diffraction prohibited the sharp stiffness gradient present at the stripe interface of mechanically-patterned hydrogels, e.g. >200 kPa/mm; only chemical initiators could create such transitions. Another common method used to create molds similar to the photoresist mold here is to etch the pattern into a glass substrate. However deep etching with hydrofluoric acid may compromise pattern sidewalls [15], thus obtaining sharp feature transitions in the resulting hydrogel cast from the mold is likely to be difficult. On the other hand once the mold is fabricated, the 2-step polymerization method used to make mechanically-patterned hydrogels can be performed rapidly and within almost any setting, aside from tuning the acrylamide concentrations appropriately for the desired stiffness.

4.2 Improving cell fate and mimicking disease

Mechanical patterns encouraged ASC elongation and alignment, perhaps in part by directing how cell tractions, which are required for fusion [7], propagated through the matrix to align myoblasts [15, 24]. The end-to-end cell orientation likely increased the probability of M- and N-cadherin contact between cells, which is required for fusion and is regulated by RhoA [26]. It has been suggested that other fusion related proteins have contractility-dependent expression, including the Rho-GTPase-activating protein (GRAF1) [42] and myoferlin [43]. Though they do not fuse, striation assembly in cardiomyocytes is also directly regulated by N-cadherin-containing structures [44], whose disruption or misalignment in an unpatterned matrix could impair assembly. Further molecular evidence supporting mechanically-patterned hydrogel mechanism is that loss of talin, which itself is a mechano-sensor [45], impairs both myoblast fusion and sarcomere assembly [46].

Mechanical patterns do not just encourage alignment, they can be used to mimic the diseased niche. Muscle related diseases, while they increase global tissue stiffness, have shown dramatic changes in local ECM stiffness from the fibrosis that they induce [15, 47,

48]. A myogenic-osteogenic mechanically-patterned hydrogel mimics the stiffer, fibrotic but heterogenous environment of dystrophic muscle [15]. Prior to *in vivo* studies with injected stem cells, sequentially culturing muscle and ASCs on a mechanically-patterned hydrogel could allow one to examine how ASCs might behave in the diseased state *in vivo*. Mechanically-patterned hydrogel may also be suitable for studies examining mechanisms behind impaired fusion with fibrotic muscle diseases. For example, it is not certain if the traction-mediated M-cadherin expression mentioned above, which likely becomes altered in the diseased state, is responsible for M-cadherin's down– and up–regulation in caveolin-3 transgenic and null cells, respectively [49]. Taken together, mechanically-patterned hydrogel is likely a suitable platform to pose a variety of muscle function questions.

4.3 Differential cell sorting for organiod culture

Differential adhesion did not occur on mechanically-patterned hydrogels, though it has been reported on other durotactic substrates [39]. However all of these substrates take advantage of the well-established observation that contractile cells exhibit a "normal" phenotype on stiffer substrates [15, 28, 29, 50]. The lack of differential adhesion here can simply be explained by our durotactic observation with C2C12 myoblasts or from the accumulation of cells treated with mitomycin C in stiffer regions of a gradient hydrogel [11]. Yet mechanically-patterned hydrogel can also use cells which prefer softer niches, e.g. neurons [38], to pattern cells of different stiffness preference. On the other hand, Tien and coworkers have used μCP to pattern different ligands where a stamp is used to selectively block protein adsorption when the substrate is bathed in a ligand [51]. While they used the stamp to also selectively place cells on their patterns, two model cell lines expressing specific integrin heterodimers may recognize a differential ligand pattern and sort themselves once plated onto the substrate; such behavior in stem cells, which undergo stiffness-mediated differentiation only on certain ligands [9], is not likely. Yet differential sorting does occur during development [20], and these substrates may serve as a strategy to recapitulate that process *in vitro* and build cultures where neurons and muscle cells can be juxtaposed to encourage intercellular signaling.

5. Conclusions

We have demonstrated here that mechanically patterned cell culture substrates, which mimic some of the spatial parameters of ECM *in vivo*, can be used to orient muscle and stem cells into favorable positions for cell fusion and striation assembly, not by preferential adhesion but rather by their ability to durotax to a prefer set of environmental conditions. Opposing this behavior are cells such as neurons, which prefer a softer niche, and these data support the development of cultures where muscle and neuron are juxtaposed with each other to form nascent junctions. Longer-term patterning required for these observations was not possible via conventional μCP on compliant hydrogels, which suggests mechanically-patterned hydrogel as an alternative when substrate stiffness is a concern for patterned cells. Mechanically-patterned hydrogel may also serve as a potential platform in which to study mechanically induced cell behaviors in diseased muscle, which may have juxtaposed regions of firm and stiff tissue, e.g. the myogenic-osteogenic mechanically-patterned hydrogel. These data support the importance of physiologically relevant mechanical guidance cues that matrix presents to cells in regulating higher order cell functions, e.g. striation and fusion.

Supplementary Material

Refer to Web version on PubMed Central for supplementary material.

Acknowledgments

This work was supported in part by the NIH via a New Innovator Award (DP02OD006460 to A.J.E.) and the Human Frontiers Science Program (RGY0064/2010 to A.J.E.). L.G.V. was supported by an NSF pre-doctoral fellowship. S.C. was supported by a pre-doctoral fellowship from the Royal Thai Government Science and Technology. K.C.K. was supported by the California Institute for Regenerative Medicine's Bridges Program (TB1-01186).

References

1. Pittenger MF, Mackay AM, Beck SC, Jaiswal RK, Douglas R, Mosca JD, et al. Multilineage potential of adult human mesenchymal stem cells. Science. 1999; 284:143–7. [PubMed: 10102814]
2. Zuk PA, Zhu M, Mizuno H, Huang J, Futrell JW, Katz AJ, et al. Multilineage cells from human adipose tissue: implications for cell-based therapies. Tissue Eng. 2001; 7:211–28. [PubMed: 11304456]
3. Atala A. Advances in tissue and organ replacement. Curr Stem Cell Res Ther. 2008; 3:21–31. [PubMed: 18220920]
4. Discher DE, Mooney DJ, Zandstra PW. Growth factors, matrices, and forces combine and control stem cells. Science. 2009; 324:1673–7. [PubMed: 19556500]
5. Vacanti JP, Langer R. Tissue engineering: the design and fabrication of living replacement devices for surgical reconstruction and transplantation. Lancet. 1999; 354(Suppl 1):SI32–4. [PubMed: 10437854]
6. Flaim CJ, Teng D, Chien S, Bhatia SN. Combinatorial signaling microenvironments for studying stem cell fate. Stem Cells Dev. 2008; 17:29–39. [PubMed: 18271698]
7. Choi YS, Vincent LG, Lee AR, Dobke MK, Engler AJ. Mechanical derivation of functional myotubes from adipose-derived stem cells. Biomaterials. 2012; 33:2482–91. [PubMed: 22197570]
8. Flaim CJ, Chien S, Bhatia SN. An extracellular matrix microarray for probing cellular differentiation. Nat Methods. 2005; 2:119–25. [PubMed: 15782209]
9. Rowlands AS, George PA, Cooper-White JJ. Directing osteogenic and myogenic differentiation of MSCs: interplay of stiffness and adhesive ligand presentation. Am J Physiol Cell Physiol. 2008; 295:C1037–44. [PubMed: 18753317]
10. Thibault MM, Hoemann CD, Buschmann MD. Fibronectin, vitronectin, and collagen I induce chemotaxis and haptotaxis of human and rabbit mesenchymal stem cells in a standardized transmembrane assay. Stem Cells Dev. 2007; 16:489–502. [PubMed: 17610379]
11. Tse JR, Engler AJ. Stiffness gradients mimicking in vivo tissue variation regulate mesenchymal stem cell fate. PLoS One. 2011; 6:e15978. [PubMed: 21246050]
12. Chen CS, Mrksich M, Huang S, Whitesides GM, Ingber DE. Geometric control of cell life and death. Science. 1997; 276:1425–8. [PubMed: 9162012]
13. McBeath R, Pirone DM, Nelson CM, Bhadriraju K, Chen CS. Cell shape, cytoskeletal tension, and RhoA regulate stem cell lineage commitment. Developmental Cell. 2004; 6:483–95. [PubMed: 15068789]
14. Kilian KA, Bugarija B, Lahn BT, Mrksich M. Geometric cues for directing the differentiation of mesenchymal stem cells. Proc Natl Acad Sci U S A. 2010; 107:4872–7. [PubMed: 20194780]
15. Engler AJ, Griffin MA, Sen S, Bonnemann CG, Sweeney HL, Discher DE. Myotubes differentiate optimally on substrates with tissue-like stiffness: pathological implications for soft or stiff microenvironments. J Cell Biol. 2004; 166:877–87. [PubMed: 15364962]
16. Falconnet D, Csucs G, Grandin HM, Textor M. Surface engineering approaches to micropattern surfaces for cell-based assays. Biomaterials. 2006; 27:3044–63. [PubMed: 16458351]
17. Engler AJ, Sen S, Sweeney HL, Discher DE. Matrix elasticity directs stem cell lineage specification. Cell. 2006; 126:677–89. [PubMed: 16923388]
18. Marklein RA, Burdick JA. Spatially controlled hydrogel mechanics to modulate stem cell interactions. Soft Matter. 2010; 6:136–43.

19. Kloxin AM, Tibbitt MW, Kasko AM, Fairbairn JA, Anseth KS. Tunable hydrogels for external manipulation of cellular microenvironments through controlled photodegradation. Adv Mater. 2010; 22:61–6. [PubMed: 20217698]
20. Engler AJ, Humbert PO, Wehrle-Haller B, Weaver VM. Multiscale modeling of form and function. Science. 2009; 324:208–12. [PubMed: 19359578]
21. Discher DE, Janmey P, Wang YL. Tissue cells feel and respond to the stiffness of their substrate. Science. 2005; 310:1139–43. [PubMed: 16293750]
22. Collinsworth AM, Zhang S, Kraus WE, Truskey GA. Apparent elastic modulus and hysteresis of skeletal muscle cells throughout differentiation. Am J Physiol Cell Physiol. 2002; 283:C1219–27. [PubMed: 12225985]
23. Georges PC, Miller WJ, Meaney DF, Sawyer ES, Janmey PA. Matrices with compliance comparable to that of brain tissue select neuronal over glial growth in mixed cortical cultures. Biophys J. 2006; 90:3012–8. [PubMed: 16461391]
24. Sen S, Engler AJ, Discher DE. Matrix strains induced by cells: Computing how far cells can feel. Cell Mol Bioeng. 2009; 2:39–48. [PubMed: 20582230]
25. Knudsen KA, McElwee SA, Myers L. A role for the neural cell adhesion molecule, NCAM, in myoblast interaction during myogenesis. Dev Biol. 1990; 138:159–68. [PubMed: 2407576]
26. Charrasse S, Comunale F, Grumbach Y, Poulat F, Blangy A, Gauthier-Rouviere C. RhoA GTPase regulates M-cadherin activity and myoblast fusion. Mol Biol Cell. 2006; 17:749–59. [PubMed: 16291866]
27. Tse JR, Engler AJ. Preparation of hydrogel substrates with tunable mechanical properties. Curr Protoc Cell Biol. 2010; Chapter 10(Unit 10):6.
28. Rajagopalan P, Marganski WA, Brown XQ, Wong JY. Direct comparison of the spread area, contractility, and migration of balb/c 3T3 fibroblasts adhered to fibronectin- and RGD-modified substrata. Biophys J. 2004; 87:2818–27. [PubMed: 15454473]
29. Engler A, Bacakova L, Newman C, Hategan A, Griffin M, Discher D. Substrate compliance versus ligand density in cell on gel responses. Biophys J. 2004; 86:617–28. [PubMed: 14695306]
30. Radmacher M. Studying the mechanics of cellular processes by atomic force microscopy. Methods Cell Biol. 2007; 83:347–72. [PubMed: 17613316]
31. Flores-Merino MV, Chirasatitsin S, Lopresti C, Reilly GC, Battaglia G, Engler AJ. Nanoscopic mechanical anisotropy in hydrogel surfaces. Soft Matter. 2010; 6:4466–70. [PubMed: 20953281]
32. Choi YS, Matsuda K, Dusting GJ, Morrison WA, Dilley RJ. Engineering cardiac tissue in vivo from human adipose-derived stem cells. Biomaterials. 2010; 31:2236–42. [PubMed: 20031204]
33. Young JL, Engler AJ. Hydrogels with time-dependent material properties enhance cardiomyocyte differentiation in vitro. Biomaterials. 2011; 32:1002–9. [PubMed: 21071078]
34. Tse JR, Engler AJ. Preparation of hydrogel substrates with tunable mechanical properties. Curr Prot Cell Bio. 2010; Chpt 10:1–16.
35. Engler AJ, Rehfeldt F, Sen S, Discher DE. Microtissue elasticity: measurements by atomic force microscopy and its influence on cell differentiation. Methods Cell Biol. 2007; 83:521–45. [PubMed: 17613323]
36. Charest JM, Califano JP, Carey SP, Reinhart-King CA. Fabrication of substrates with defined mechanical properties and topographical features for the study of cell migration. Macromol Biosci. 2012; 12:12–20. [PubMed: 22021131]
37. Lo CM, Wang HB, Dembo M, Wang YL. Cell movement is guided by the rigidity of the substrate. Biophys J. 2000; 79:144–52. [PubMed: 10866943]
38. Flanagan LA, Ju YE, Marg B, Osterfield M, Janmey PA. Neurite branching on deformable substrates. Neuroreport. 2002; 13:2411–5. [PubMed: 12499839]
39. Gray DS, Tien J, Chen CS. Repositioning of cells by mechanotaxis on surfaces with micropatterned Young's modulus. J Biomed Mater Res A. 2003; 66:605–14. [PubMed: 12918044]
40. Zaari N, Rajagopalan P, Kim SK, Engler AJ, Wong JY. Photopolymerization in microfluidic gradient generators: Microscale control of substrate compliance to manipulate cell response. Advanced Materials. 2004; 16:2133.

41. Isenberg BC, Dimilla PA, Walker M, Kim S, Wong JY. Vascular smooth muscle cell durotaxis depends on substrate stiffness gradient strength. Biophys J. 2009; 97:1313–22. [PubMed: 19720019]

42. Doherty JT, Lenhart KC, Cameron MV, Mack CP, Conlon FL, Taylor JM. Skeletal muscle differentiation and fusion are regulated by the BAR-containing Rho-GTPase-activating protein (Rho-GAP), GRAF1. J Biol Chem. 2011; 286:25903–21. [PubMed: 21622574]

43. Doherty KR, Cave A, Davis DB, Delmonte AJ, Posey A, Earley JU, et al. Normal myoblast fusion requires myoferlin. Development. 2005; 132:5565–75. [PubMed: 16280346]

44. Goncharova EJ, Kam Z, Geiger B. The involvement of adherens junction components in myofibrillogenesis in cultured cardiac myocytes. Development. 1992; 114:173–83. [PubMed: 1576958]

45. del Rio A, Perez-Jimenez R, Liu R, Roca-Cusachs P, Fernandez JM, Sheetz MP. Stretching single talin rod molecules activates vinculin binding. Science. 2009; 323:638–41. [PubMed: 19179532]

46. Conti FJ, Monkley SJ, Wood MR, Critchley DR, Muller U. Talin 1 and 2 are required for myoblast fusion, sarcomere assembly and the maintenance of myotendinous junctions. Development. 2009; 136:3597–606. [PubMed: 19793892]

47. Berry MF, Engler AJ, Woo YJ, Pirolli TJ, Bish LT, Jayasankar V, et al. Mesenchymal stem cell injection after myocardial infarction improves myocardial compliance. Am J Physiol Heart Circ Physiol. 2006; 290:H2196–203. [PubMed: 16473959]

48. Stedman HH, Sweeney HL, Shrager JB, Maguire HC, Panettieri RA, Petrof B, et al. The mdx mouse diaphragm reproduces the degenerative changes of Duchenne muscular dystrophy. Nature. 1991; 352:536–9. [PubMed: 1865908]

49. Volonte D, Peoples AJ, Galbiati F. Modulation of myoblast fusion by caveolin-3 in dystrophic skeletal muscle cells: implications for Duchenne muscular dystrophy and limb-girdle muscular dystrophy-1C. Mol Biol Cell. 2003; 14:4075–88. [PubMed: 14517320]

50. Thomas TW, DiMilla PA. Spreading and motility of human glioblastoma cells on sheets of silicone rubber depend on substratum compliance. Med Biol Eng Comput. 2000; 38:360–70. [PubMed: 10912355]

51. Tien J, Nelson CM, Chen CS. Fabrication of aligned microstructures with a single elastomeric stamp. Proc Natl Acad Sci U S A. 2002; 99:1758–62. [PubMed: 11842197]

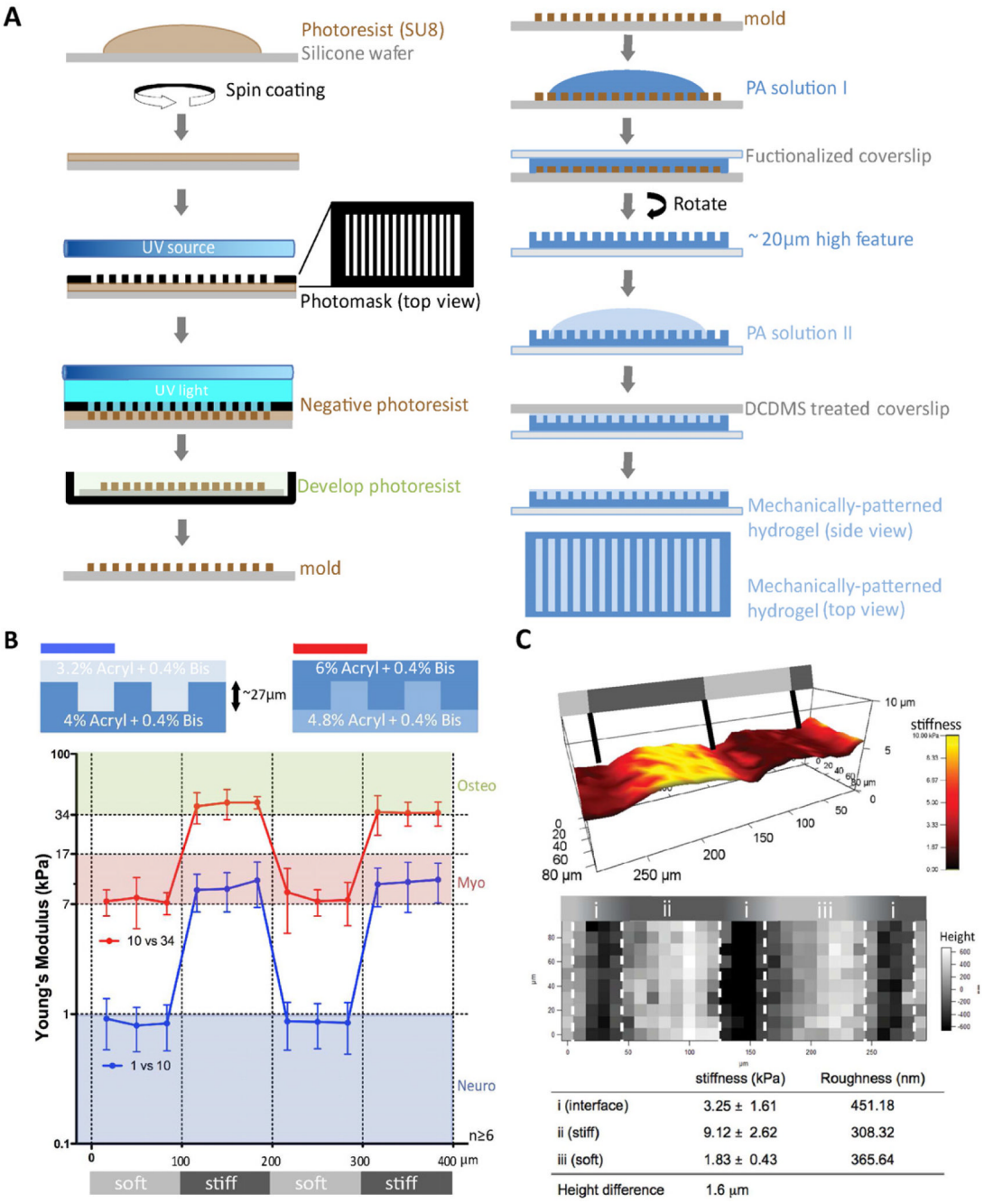

Figure 1. Mechanically-patterned hydrogel fabrication and characterization

(A) Schematic of photolithography and 2-step polyacrylamide gel fabrication. (B) Matrix stiffness (bottom) was measured for neurogenic-myogenic (blue) and myogenic-osteogenic (red) mechanically-patterned hydrogels (n≥6) fabricated using the indicated polyacrylamide concentrations for top and bottom hydrogels (top). Light and dark gray regions in the bottom schematic represent soft and stiff regions, respectively. (C) Matrix stiffness, height, and surface roughness of mechanically-patterned hydrogels were visualized with three adjacent 90 μm × 90 μm force maps. Matrix stiffness of adjacent soft and stiff strips was overlaid with surface height in a 3D reconstruction of the surface features (top). 2D height topography is shown individually (middle). Values for stiffness and roughness are shown for

stiff and soft stripes as well as the interface. Overall height difference was also computed and shown. Light and dark gray regions in the schematics represent soft (1 kPa) and stiff (10 kPa) regions, respectively.

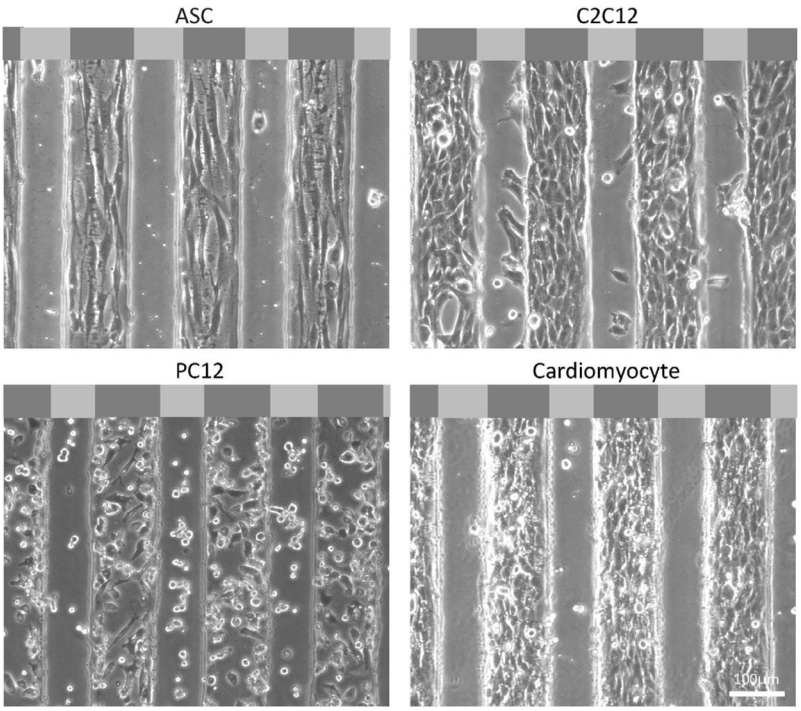

Figure 2. Cell adhesion preference

Different cell types preferentially localized to the stiffer regions of the neurogenic-myogenic mechanically-patterned hydrogels after 48 hours in culture. Phase contrast images show representative images with very confluent cells on the stiffer myogenic lanes for ASC, C2C12, and chicken cardiomyocytes. A portion of the PC12s remained less well-spread and adherent on the softer neurogenic stripes. Light and dark gray regions in the schematic at the top of each image represent soft (1 kPa) and stiff (10 kPa) regions, respectively.

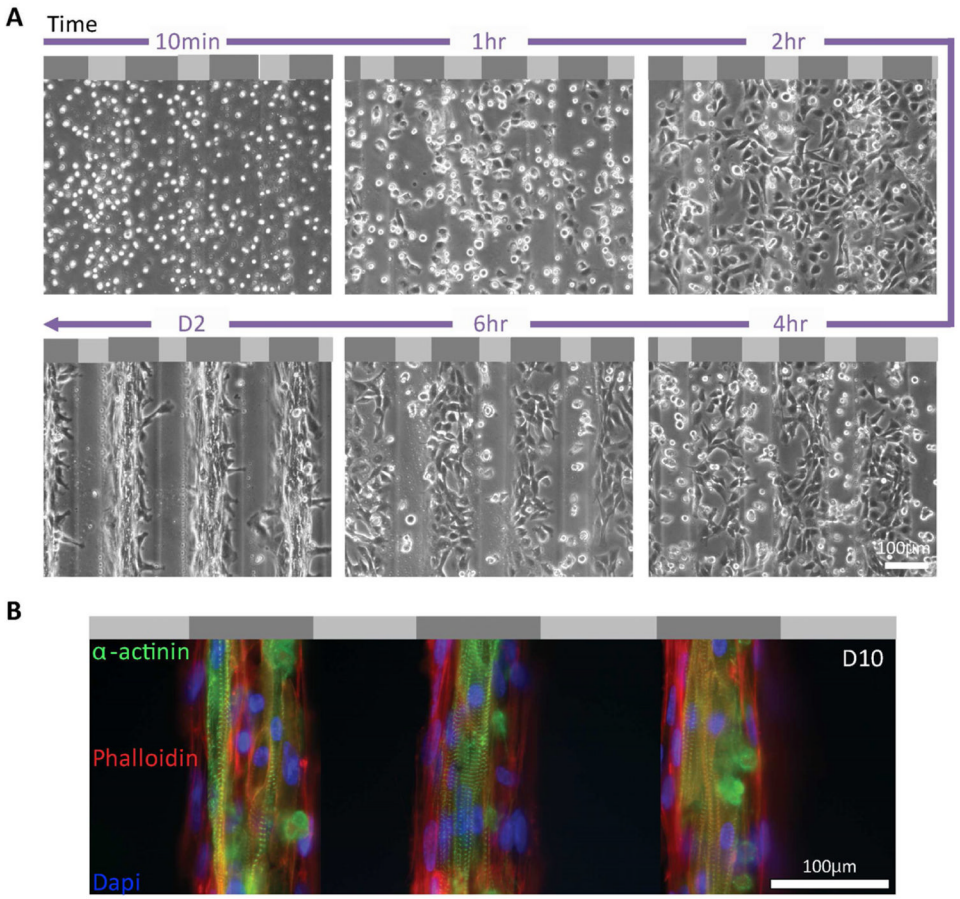

Figure 3. Attachment and alignment of cardiomyocytes on neurogenic-myogenic mechanically-patterned hydrogel

(A) Time lapse images of chicken cardiomyocyte attachment to neurogenic-myogenic mechanically-patterned hydrogel showed adhesion and preferential migration and spreading on stiffer myogenic stripes. Light and dark gray regions in the schematic at the top of each image represent soft (1 kPa) and stiff (10 kPa) regions, respectively. (B) Three consecutive myogenic stripes were fluorescently stained by rhodamin-phalloidin (red), α–actinin (green), and DAPI (blue), revealing an aligned network of cardiomyocytes on myogenic stripes of mechanically-patterned hydrogel at day 10 with adjacent myofibroblasts that lack α–actinin.

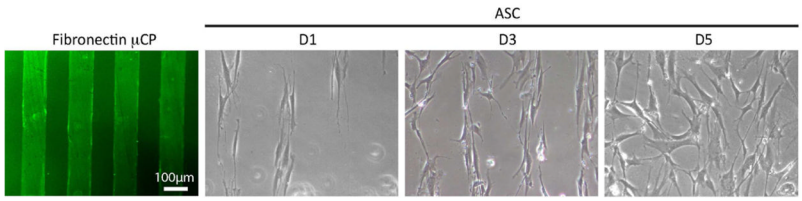

Figure 4. ASC on fibronectin-microcontact printing

μCP was confirmed by anti-fibronectin staining (right). ASCs recognized pattern initially at day 1 and proliferated and aligned on pattern at day 3, however, pattern was failed from day 5 and cells attached on both printed and non-printed area.

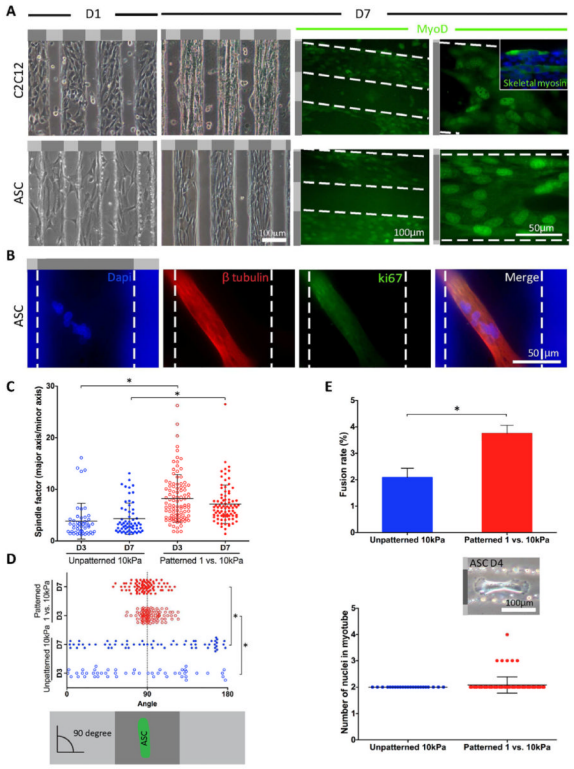

Figure 5. Mechanically-patterned hydrogel enhances myotube fusion of ASC

(A) Representative cell alignment on neurogenic-myogenic mechanically-patterned hydrogels at day 1 and 7 for both C2C12 and ASCs shown in phase contrast (top) and with MyoD staining at day 7 (bottom). Inset image shows C2C12 myoblasts, which further differentiated into skeletal fast myosin-expressing myotubes. White dashed lines indicate the edges of each region of mechanically-patterned hydrogel. (B) Representative multi-nucleated myotube stained with Dapi that was identified with β-tubulin (red) and negative for ki-67 staining (green), which is indicative of quiescent cells. (C) Spindle factor from ASCs on mechanically-patterned hydrogel were significantly greater than those on unpatterned 10 kPa PA hydrogels at both day 3 and 7. (D) To show the alignment of ASCs on gels, cell angle was measured by phalloidin staining (90° = perfectly aligned on mechanically-patterned hydrogel). ASCs on mechanically-patterned hydrogel showed higher level of alignment that those on unpatterned 10 kPa PA hydrogels at day 7. (E) A higher fusion rate was observed on the mechanically-patterned hydrogel compared to unpatterned 10 kPa PA gels (top) [7]. The number of nuclei per mechanically-patterned hydrogel or unpatterned hydrogel myotube was also quantified (bottom). The inset image shows characteristic multi-nucleated myotube in phase contrast. Light and dark gray regions in the schematic next to or on top of each image represent soft (1 kPa) and stiff (10 kPa) regions, respectively. *p <0.05 for all indicated comparisons.